Study of the Cyclists' Skin Deformation for Compression Skinsuit Design

Abstract

Skin deformation during cycling is an important factor when designing a performance cycling garment as the space between the body and the garment creates aerodynamic drag and subsequent negative impact on the cyclist's performance. Thus, the skin deformation has been studied for an aerodynamic skinsuit via the three-dimensional (3D) body image. An understanding of the skin deformation during cycling, especially at the torso and thigh areas are essential for the cycling suit design and pattern making, and a few studies investigating this.

This study aimed to analyze the cyclists' 3D skin deformation during cycling captured by a motion capture system. Eight healthy male amateur cyclists were invited to participate in this study. The trajectories of sixty-eight reflective markers on the skin were continuously captured during cycling. The mean values and standard deviations of the eight participants' skin deformation were analyzed against the static posture skin data. The results showed that the anterior torso skin was contracted by 0.3% - 22.3%, while most of the posterior torso skin measurements were expanded by 6.7% - 32.0% during cycling in bending posture when compared with standing posture during cycling. The skin deformation value of the torso was stable after first bending posture during cycling. The thigh skins were deformed from -14.7% to 7.6% during cycling. The results can be used as pattern adjustment rate for compression cycling skinsuit design.

Keywords: motion capture, skin deformation, cycling, compression, skinsuit

Introduction

A compression cycling skinsuit (CCS) was found to decrease the aerodynamic drag by 30% when compared with shorts and jersey top during cycling (1), whilst cycling performance can be improved due to the reduction of the aerodynamic drag by wearing a skinsuit during 25-mile road cycling (2). Clothing fit for the CCS is essential because it determines the amounts of wrinkles and size of wake (e.g., airdrag) during cycling, which sequentially affects the cycling performance and the aerodynamic drag (3-5). Ease amount is one of the essential parameters for garment fitting (6). Over or less negative ease amounts of the CCS pattern will induce over-compression or a thicker air gap between garment and skin to increase more air drag during cycling. Therefore, it was considered necessary to study the skin deformation during cycling.

Previous studies involved compression tight-fitting clothes design and pattern development with the data measured by means of three-dimensional (3D) body scanning technology. Choi and Ashdown (7) investigated the hip and leg skin deformation of 25 young females in three static postures (i.e., 120° knee flexion posture, stepping posture, and sitting posture with 90° knee flexion) and suggested to apply the skin deformation changes for tight-fitting clothes pattern design. Lee's research group (8) compared skin deformation for the leg in both a squatting posture and standing posture for outdoor tight-fitting pants design. Seo et al. (9) used 3D body scanning to scan and analyze the skin deformation of legs in four different knee flexion angles (i.e., 0°, 30°, 45°, and 60°). Choi and Hong (10) compared the skin deformation with the method, which was similar with Seo (9), for tight-fitting leggings pattern development. These studies have shed light on the studies of skin deformation during movement for tight-fitting sportswear design. However, the fitting status at a specified body part would be affected by the localized skin deformation during different motions (11). Aforementioned results from previous studies hardly applied for CCS design. For CCS development, pedal forces, saddle height, and kinematic consideration should be considered (12) which were missed in previous studies.

Earlier investigations indicated that changes in skin deformation and pedal force production were related to saddle height (3). The force production and magnitude of joint load depended on muscle length which affected skin deformation and varied during dynamic cycling (13, 14). Skin deformation analysis in a static position,

measured by 3D scanner, cannot accurately represent the kinematics during dynamic motion (14, 15). It is essential to the study of accurate skin deformation that factors such as pedal forces, saddle height, and kinematic consideration are taken into account in a continuous dynamic motion for negative ease amounts adjustment of CCS pattern and aerodynamic function improvement.

Skin is important to the function of the mechanics of the body, for example, skin can transmit external forces on the locomotor system. Skin deformation distributes the effect of forces over large area of contact to different body parts or joints, and it can also attenuate peak forces, which subsequently influences the sport performance (16). As a consequence, designers must consider the effects of skin deformation when designing sportswear. However, the skin deformation analysis of the torso is limited. A rider's upper body posture has the largest contribution to aerodynamic drag during cycling (4, 14, 17). Balasubramanian (18) found that the upper body posture affects the lower limb muscle functions of cyclists during cycling while bending posture is preferred by cyclists for speed enhancement and reduction of energy use. However, few studies have investigated the skin deformation of a torso in a bending posture during cycling and the application of the aforementioned theory into the functional design of CCS. Thus, the aim of this study was to investigate the skin deformation of the torso and thigh of the cyclists during dynamic cycling in a bending posture, hence suggesting the optimum negative ease amounts for the CCS pattern to improve aerodynamic and support better muscle movement. Factors influencing the cycling performance including pedal forces, saddle height, and kinematic were considered in this study.

Methods

Subjects

A total of eight amateur male cyclists with over six-year cycling experience were invited to participate in this study. The participants were informed of the experimental procedures and signed a consent form before the experiment. Human participant ethics approval was granted by The XXX University Ethics Committee (HSEARS20180606002). The body measurements are shown in Table 1. According to their height and chest circumference, the participants were divided into three size groups: 170/90 (A), 170/96 (B), and 175/95 (C) (19).

Table 1. Body measurements of subjects.

Measurements	Subjects									
	1	2	3	4	5	6	7	8	Mean	S.D
Age (year)	23.5	24.5	28	25	25	26.5	23	24.5	25.0	1.5
Size group	C	A	C	B	B	A	A	C		
Height (cm)	176	173	177	168	170	168	168	181	171.6	5.0
Weight (kg)	63.5	54.5	66	63.1	70	69	64.8	67.3	64.8	4.5
Body mass index (kg/m²)	21.5	18.5	23.9	22.9	22.5	23	23	20.8	22.0	1.6
Neck circumference (cm)	46.5	38.3	46.8	44.2	46.4	44.1	43	42	43.9	2.7
Chest circumference (cm)	101	86	92	95	99	92	90	86	92.6	5.1
Waist circumference (cm)	83	74	83	82	89.7	82	79	75	81.0	4.7
Hip circumference (cm)	99	93	97	96.7	97	97.5	97	97	96.8	1.6
Back shoulder width (cm)	51.3	40	44.4	48.6	46.4	43.1	42.5	44	45.0	3.4
Front shoulder width (cm)	44.3	39.1	42	41	41.4	39.4	42	41	41.3	1.5
Mid-thigh circumference (cm)	48	45	46.4	44.6	50.2	46.5	46	45	46.5	1.7
Knee circumference (cm)	35.2	35.4	37.6	35	36.6	39.1	35.8	35	36.2	1.4
Front center length(cm)	44	42	43	41	40.8	40	41	46	42.23	1.9
Back center length (cm)	50	48.5	49	46	46.5	46	46	52	48.0	2.1
Crotch length (cm)	30	29.8	28.8	28.8	29.6	26.1	27.9	30.9	29.0	1.4

Apparatus

Round reflective markers of 15mm in diameter and 1.81g in weight were attached on the skin, and data were continuously captured in 3D space by a twelve resolution (1280*1024) and speed (up 2kHz) digital cameras motion capture system (Eagle, Motion Analysis Corporation, USA). The capturing frequency was 90Hz. The system error was less than 2mm. The stationary 700C road bicycle (X-Treme, Foshan, China) was used for cycling in the study.

Landmarks and body dimensions

Definition of sixty-eight landmarks (Table 2, Figure 1) were attached on subjects' skin according to the motion capture landmark and the anthropometric landmark protocol

(20-23). Three 10mm width, 1mm thickness elastic straps were placed on the upper chest, waist, and hip circumferences separately to facilitate to find out main landmarks (e.g., landmark No. 26, 27, 40, 41) from the body. The strap on the upper chest should lay across the anterior and posterior axilla points (20), then the second strap across the narrowest part of the waist (24). The third strap on the hip circumference should lay across the buttock points (23). Each strap was placed at a transverse level from two sides of views. These three straps were removed after all landmarks were attached on the skin.

Table 2. Definition of landmarks.

Landmark Number	Landmark Definition	Reference
1	The top center of parietal bone and vertical to the posterior center line	(22)
2	The center of occipital bone and vertical to the posterior center line	(20)
3, 4	Side neck point, L/R	
5	Spinous process of the 7th cervical vertebrae	
6	Sternum jugular notch	
7, 8	Acromioclavicular joint, L/R	
9, 10	The middle point between 3 and 7, 4 and 8	(22)
11	The middle point between 9 and 10	
12	The middle point between 7 and 8 at the horizontal line	
13, 14	The middle point between 7/8 and 12 at the horizontal line	
15, 16	Greater tubercle, L/R	
17, 18	Axilla point post, L/R	
19	The middle point between 17 and 18 at the horizontal line	
20, 21	The inferior angle point of the scapula, L/R	
22	Mesosternale	
23, 24	The middle point between mesosternale and axilla point ant., L/R	
25	Waist level	(24)
26, 27	Side point on waist level, L/R	
28, 29	Middle point between side point (26/27) and 25, L/R	
30	T12 on the waist level	
31, 32	Middle points between L/R side point and T12 on the waist level	
33, 34	Lower third of shoulder and elbow, L/R	

35, 36	Point of trochiea, L/R	(20)
37, 38	Lateral epicondyle point, L/R	
39	5cm vertically below the umbilicus point, abdominal ext. level	
40, 41	Iliocristale, L/R	
42, 43	The middle point between the iliocristale (L/R) and 39 at transvers level	
44	The middle point between L and R iliocristale	
45, 46	The middle point between L/R iliocristale and point 44	
47, 48	Trochanterion, L/R	(21)
49, 50	Femur lateral epicondyle, L/R	
51, 52	Center point of patella, L/R	
53, 54	Intercondylar fossa point at knee level, L/R	
55, 56	The middle point between trochanterion and femur lateral epicondyle, L/R	
57, 58	Ant. TMax-max thigh point, L/R	
59, 60	Post. TMax-max thigh point, L/R	
61, 62	lateral malleolus L/R	
63, 64	The middle point between femur lateral epicondyle and lateral malleolus	
65, 66	Ant. middle point of tibia, L/R	
67, 68	Post. middle point of tibia, L/R	

L: left, R: right.

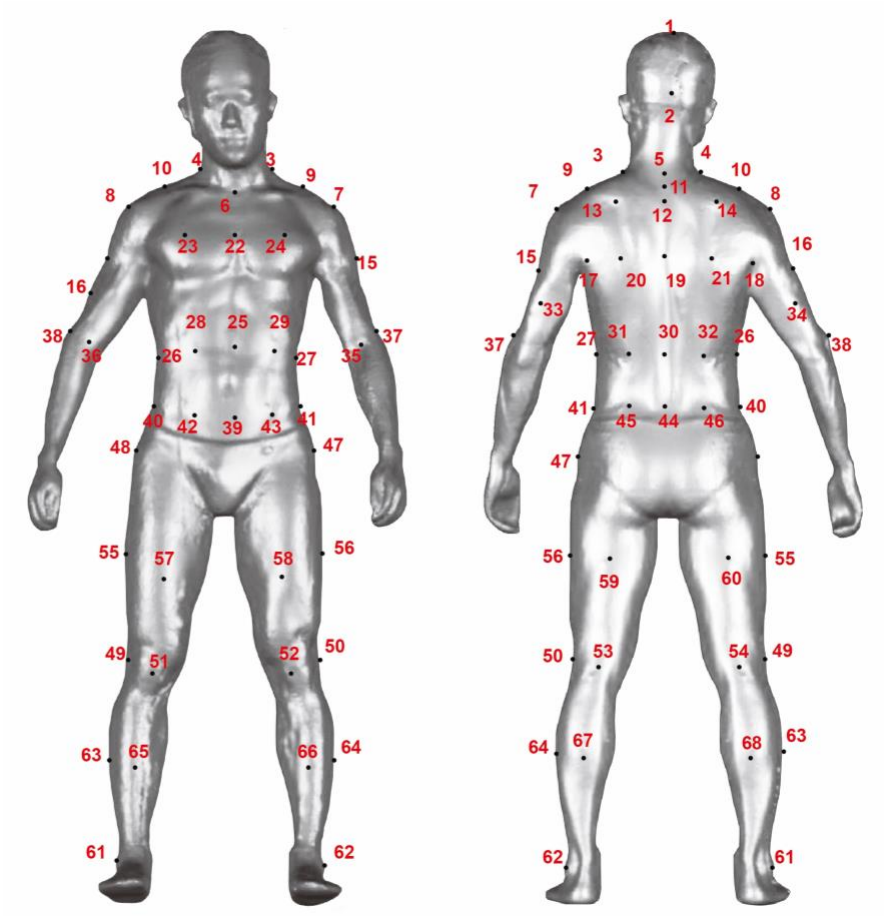

Figure 1. Sixty-eight landmarks

Thirty-one body dimensions (Table 3) were measured from the anterior and posterior torso, and thigh, which are collected as reference for garment pattern making (10, 25). Each of the body dimensions was defined using two or more of the evaluated landmarks.

Table 3. Thirty-one anthropometric dimensions were measured.

ID	Measurement item	Relate landmark	ID	Measurement item	Relate landmark
A'	Ant. center L	6, 22, 25, 39	**A**	Post. center L	5,11, 12, 19, 30, 44
B'	Middle side L of anterior	10, 23, 28, 42	**B:**	Post. Middle side L of posterior	10, 14, 21, 32, 46
C'	Anterior side L	8, 26, 40	**C**	Posterior side L	8, 18, 26, 40
D'	Ant. neckbase C	3,6,4	**D**	Post. neckbase C	3, 5, 4
E'	Ant. biacromial W	8, 6, 7	**E**	Post. biacromial W	8, 14, 12, 13, 7
F'	Half ant. upper chest L	23, 22, 24	**F**	Post. interscye L	17, 20, 19, 21, 18

G'	Ant. waist C	26, 28, 25, 29, 27	**G**	Post. waist C	27, 31, 30, 32, 26
H'	Ant. pant waist aC	40, 42, 39, 43, 41	**H**	Post. pant waist C	41, 45, 44, 46, 40
J'	Ant. neck point to side waist point L	4, 22, 29, 41	**J**	Post. neck point to side waist point L	4, 19, 31, 41
K'	1/2 shoulder point to 1/4 ant. pant waist point, crossing the upper chest point and 1/2 ant. waist point	10, 23, 25, 43	**K**	1/2 shoulder point to post. 1/4 pant waist point, crossing the scapula point and 1/2 post. waist point	10, 21, 30, 45
L'	Acromioclavicular point to center point of ant. pant waist, crossing 1/4 waist point	8, 28, 39	**L**	Acromioclavicular point to center point of post. pant waist, crossing 1/4 waist point	8, 32, 44
M'	Side waist point to 1/4 side point of ant. pant waist	26, 42	**M**	Side waist point to 1/4 side point of post. pant waist	26, 46
LB	Post. TMax-max thigh to the knee L	59, 53	**LA**	H-max hip to knee L	48, 55, 49
LD	1/2 TMax-max thigh G	57, 55, 60	**LC**	Ant. TMax-max thigh to the knee L	57, 51
LF	Ant. TMax-max thigh point to Trochanterion point to post. TMax-max thigh point	57, 48, 60	**LE**	1/2 knee G	51, 49, 54
			LG	Center point of patella to TMax-max thigh side point to Intercondylar fossa point	51, 55, 54

Ant.: anterior; C: circumference; G: girth; L: length; Post: posterior; W: width.

Procedure

The motion capture system was calibrated before the experiment. When the participants arrived at the laboratory, the reflective markers were attached to the skin of participants who wore only briefs and sport shoes. Each participant was captured in a standing posture for ten seconds (Figure 2(a)) before capturing the cycling motion in a bending

posture (Figure 2(b)). Then, the participants sat on the road cycling bicycle and the saddle height was adjusted according to the knee angle method (12), using the knee flexion angle which was 25 - 30 degrees, and the top of the handlebar to the saddle height which was 2 inches (26). Each subject cycled for two minutes, three times, a in bending posture with torso flex of 60 degrees. The participants were asked to cycle at a metronomic pace to keep the pedaling speed at 60 revolutions per minute consistently and guarantee the accuracy of the obtained data.

Analysis of skin deformation during cycling in bending posture

Optical tracking marker information was converted to skeleton (Figure 2(a') and (b')). The skin deformations of thirty-one body dimensions in a static position and during cycling were compared and analyzed.

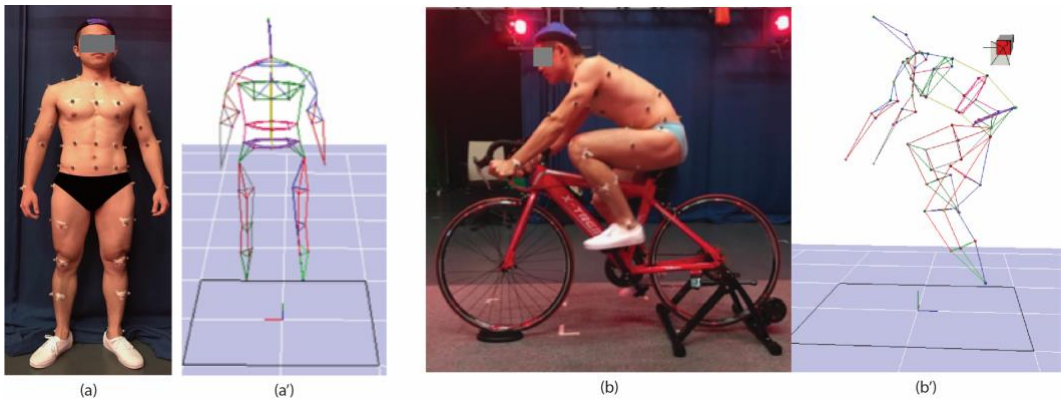

Figure 2. Static standing (a & a') & cycling in a bending (b & b')

3D skin deformation was calculated at transverse, longitudinal and diagonal directions by Equation (8) when the subjects peddled from the top dead center (TDC) to the bottom dead center (BDC) (Figure 3) (27).

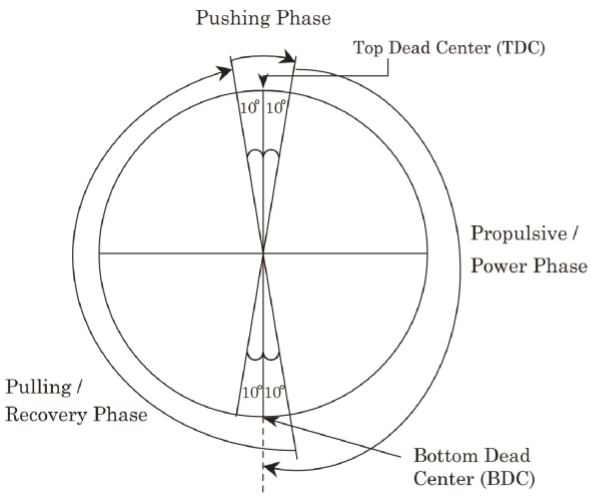

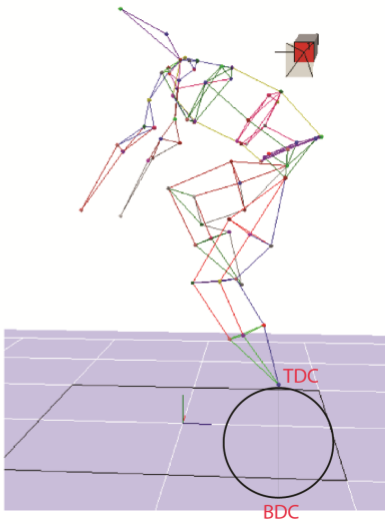

Figure 3. Peddle from the TDC to the BDC

The skin contraction and extension of eight subjects were averaged out, showing with mean value and standard deviation (SD) (i.e., mean (SD)). To analysis the skin deformations of the thigh and the torso in Table 3 for eight subjects in each degree of one cycle (i.e., from TDC to BDC) during cycling, the interpolation was used to ensure the length of the capturing data in each cycle consistently by Matlab r2018a (Mathworks corp., USA). Total 361 points length in each cycle ranged from 0 to 360 degree (Equation 1).

$$\text{Skin deformation rate\%} = \frac{L_{cycling} - L_{standing}}{L_{standing}} \times 100\% \qquad \text{Equation 1}$$

$L_{cycling}$, length of anthropometric dimension during dynamic cycling in bending posture.
$L_{standing}$, length of anthropometric dimension during static standing posture.

Results

Through the skin deformation analysis of male amateur cyclists by motion capture system, it was found that the maximum skin contraction was observed at the anterior torso and posterior thigh, and the minimum skin contraction was observed at the posterior and anterior thigh according to the Equation. Although each participant showed different skin deformation values due to the difference in their sizes, the skin deformation trends were similar in pattern.

Skin deformation of the torso

The skin deformation range of the anterior (A' - M') and posterior torso (A - M) was from -30% to 35% during cycling in bending posture, while most of skin lines of the anterior and posterior torso were deformed oppositely (see Figure 4). The deformation rate of each skin line on the torso in three directions was maintained at a consistent level from the beginning (TDC) to the end (TDC) during cycling.

From the longitudinal skin deformation analysis (See A - C or A' - C' in Figure 4), the skin deformation of maximum compression was placed at the anterior centerline of A' (-14.2% (6.8%), while the skin deformation of maximum elongation was placed at the posterior centerline of A (9.3% (9.2%)) when compared with standing posture.

From the transverse skin deformation analysis (See D - H or D' - H' in Figure 4), the anterior skin lines of neck circumference (D'), shoulder length (E'), and 1/2 chest (F') were decreased, while the posterior skin lines of neck circumference (D), shoulder length (E), and posterior length (F) were increased during cycling in a bending posture. The skin deformation of maximum contraction was located at the E' and was contracted by 18.7% (5.1%), while the skin deformation of maximum expansion was located at F and was expanded by 32.0% (7.9%) in a transverse direction of the body during cycling.

From the diagonal analysis (See I - L or I' - L' in Figure 4), the skin deformation of maximum shrinking was at the anterior sideline (L') and was shrunk by 22.3% (5.3%). Correspondingly, the skin deformation of maximum elongation was at the posterior sideline (L) and was elongated by 22.9% (7.6%) in the diagonal direction during cycling. The maximum skin deformation was at two sides of the torso, while the minimum skin deformation was at the center of the torso (H, I, H', and I') in the diagonal direction during cycling.

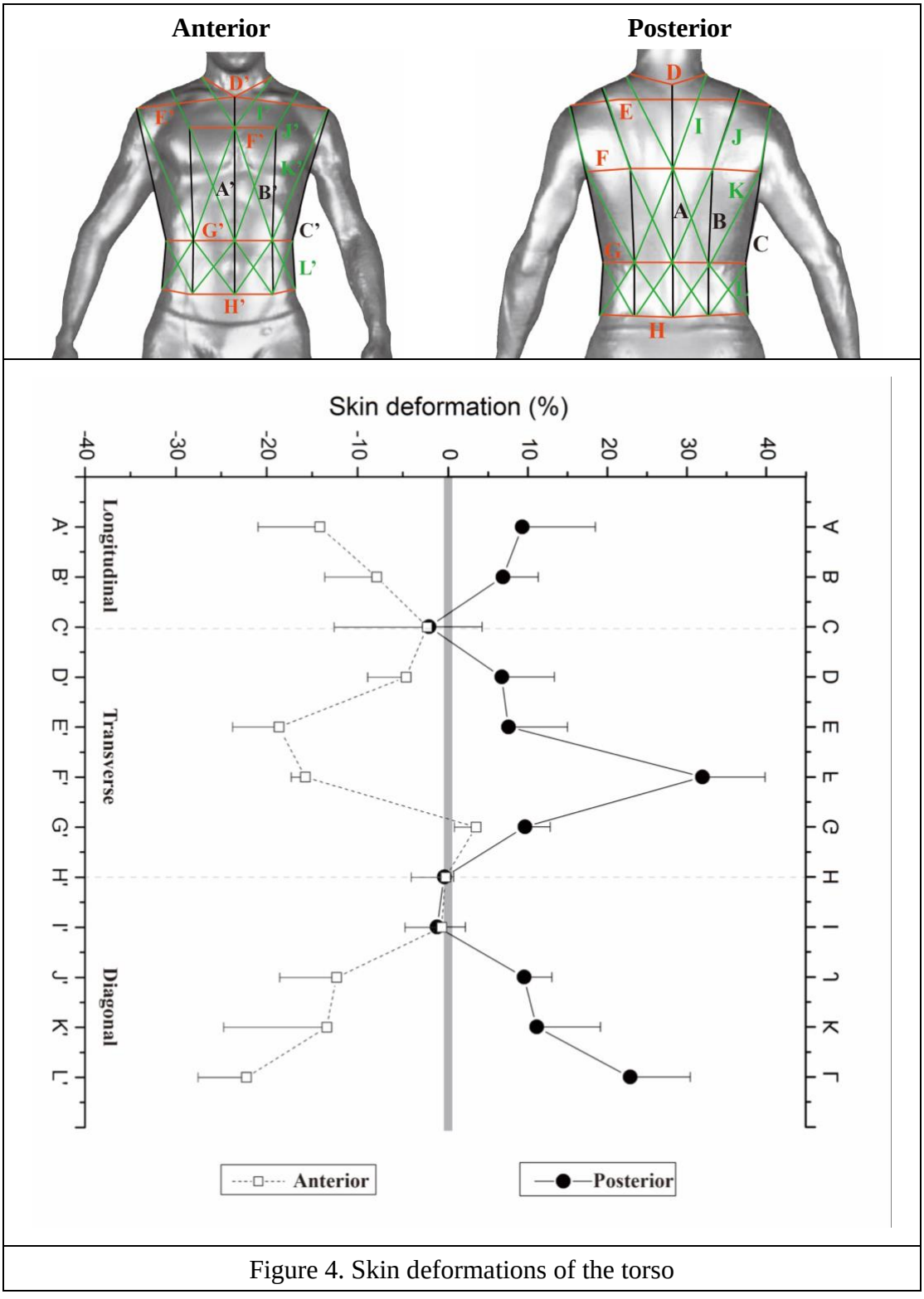

Figure 4. Skin deformations of the torso

Skin deformation of the thigh during cycling

Figure 5 shows the mean results of dynamic skin deformation of the thigh of eight subjects in three directions during cycling from TDC to BDC to TDC. The averaged knee angle of eight subjects' was 73 ° at TDC and 137 ° at BDC during cycling. The

skin deformation of the thigh (LA-LG) was changed inversely proportional to the knee angle during cycling. The change rates of the skin deformation of the thigh (LA-LG) reached or were close to the non-extension zone when subjects pedaled at the BDC position with the maximum knee angle. The skin deformation rates of the thigh reached their peak when the subjects pedaled at TDC with the minimum knee angle. The skin deformation range of the thigh was between 17.5% and -25.0% during cycling.

The maximum contraction of the thigh, which was LB, was contracted by 14.7%, while the maximum extension was LC which was extended by 7.6% during cycling. The skin deformed more at the knee circumference (LE) than at the middle of the thigh circumference (LD).

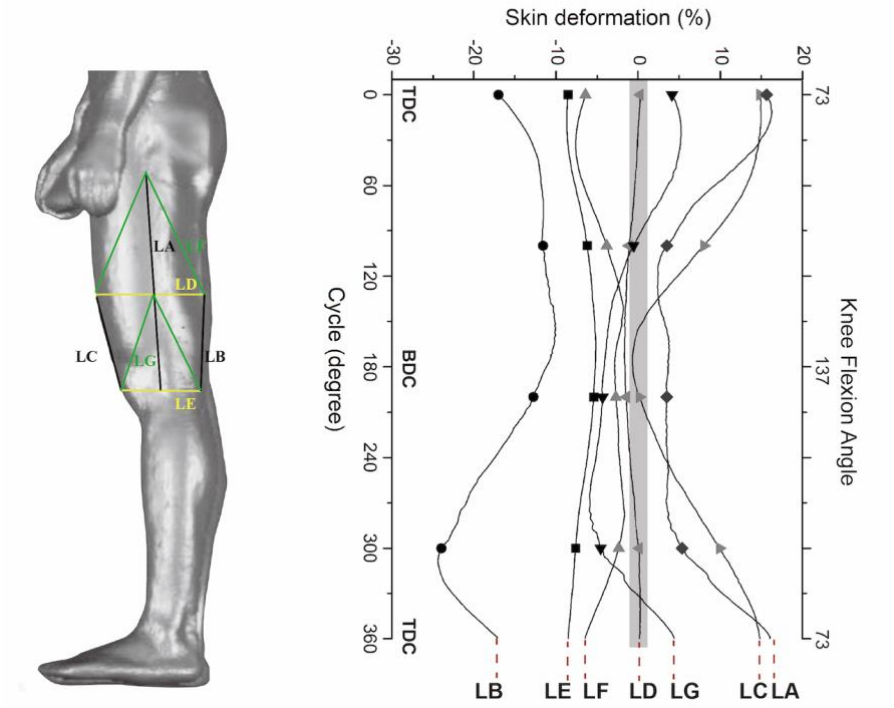

Figure 5. Skin deformations of the thigh

Skin deformation application on CCS pattern adjustment

The CCS pattern was adjusted based on the results of the skin deformation comparison between cycling in bending posture and static standing posture by motion capture system. The results of mean skin deformation rates were applied for the CCS pattern adjustment for the cyclists to cycle in a bending posture. The dotted lines in the figures (from Figures 6 to 11) indicate the CCS pattern constructed from standing posture

measurements, and the solid lines in figures indicate the modified CCS pattern based on skin deformation rates from 3D motion capture results. 20% of negative ease was applied for compression power generation. The pattern was adjusted according to the Equation 2 below. The ease rate applied for pattern adjustment was defined as 0% when skin deformation rate range was equal to or smaller than 0.5% during cycling in a bending posture. Figures 6-11 show the examples of pattern development for 170/90 (A) size.

$$\text{Ease rate\%} = (L_{\text{standing}} * 80\%) +/- (L_{\text{standing}} * 80\%) * \text{Skin deformation\%} \quad \text{Equation 2}$$

$L_{standing}$, length of anthropometric dimension during standing posture. 80% indicates 20% of negative ease.

Longitudinal adjustment rates of the CCS pattern

For longitudinal direction adjustment rates, according to the results shown in Table 4, most of skin lines at posterior torso (e.g., A and B) were increased, while the skin at anterior torso (e.g., A' and B') were decreased.

Table 4. Longitudinal direction analysis for the ease rate of CCS torso pattern.

Items	ID	Skin deformation (%)	Ease rate (%)
Ant. center L	A'	-14.2	(Ant. center L * 80%) – (Ant. center L * 80%) * 14.2%
Post. center L	A	9.3	(Post. center L* 80%) + (Post. center L* 80%) * 9.3%
Ant. middle side L	B'	-7.9	(Ant. middle side L * 80%) – (Ant. middle side L * 80%) * 7.9%
Post. middle side L	B	6.8	(Post. middle side L * 80%) + (Post. middle side L * 80%) * 6.8%
Ant. side L	C'	-2.3	(Ant. side L * 80%) - (Ant. side L * 80%) * 2.3%
Post. side L	C	-2.5	(Post. side L * 80%) - (Post. side L * 80%) * 2.5%

Ant.: anterior; H: height; L: length; Post.: posterior.

Posterior length

After the skin deformation analysis between landmarks, it was found that the maximum deformation of the posterior center length (A) was placed between landmark points 30 and 40. Instead of simply increasing the whole posterior center length (A), the increased skin deformation was added at point 30 - 40 on the pattern (see Figure 6). For the posterior middle side length of posterior (B), and the largest skin deformation occurred at 32 - 46 parts, which was reflected on the pattern as shown in Figure 6.

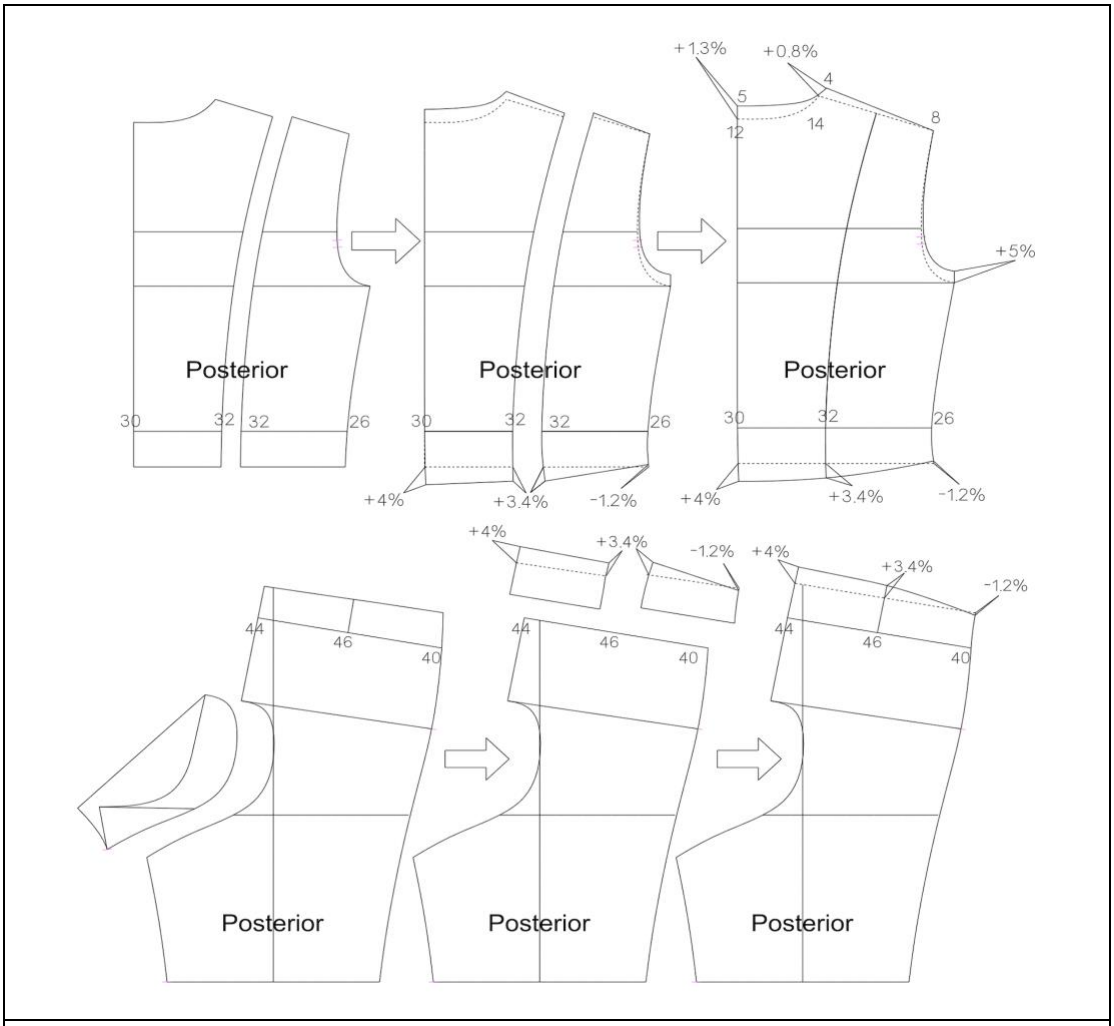

Figure 6. Longitudinal adjustment of ease rates for the CCS posterior pattern

Solid line, the adjusted CCS pattern.

Collar height

From the landmark-by-landmark analysis, the skin deformation between point 5 and 12 was increased by 1.3%, and the skin deformation between side neck point of 4 and 14 was increased by 0.8% (Figure 6).

Anterior length

The largest skin deformation of anterior center length (A) was decreased between landmark points 25 and 39, decreased by 7.1% for the CCS pattern adjustment. Similarly, the middle side length of anterior (B') was decreased by 3.9% when transformed on the CCS pattern (Figure 7).

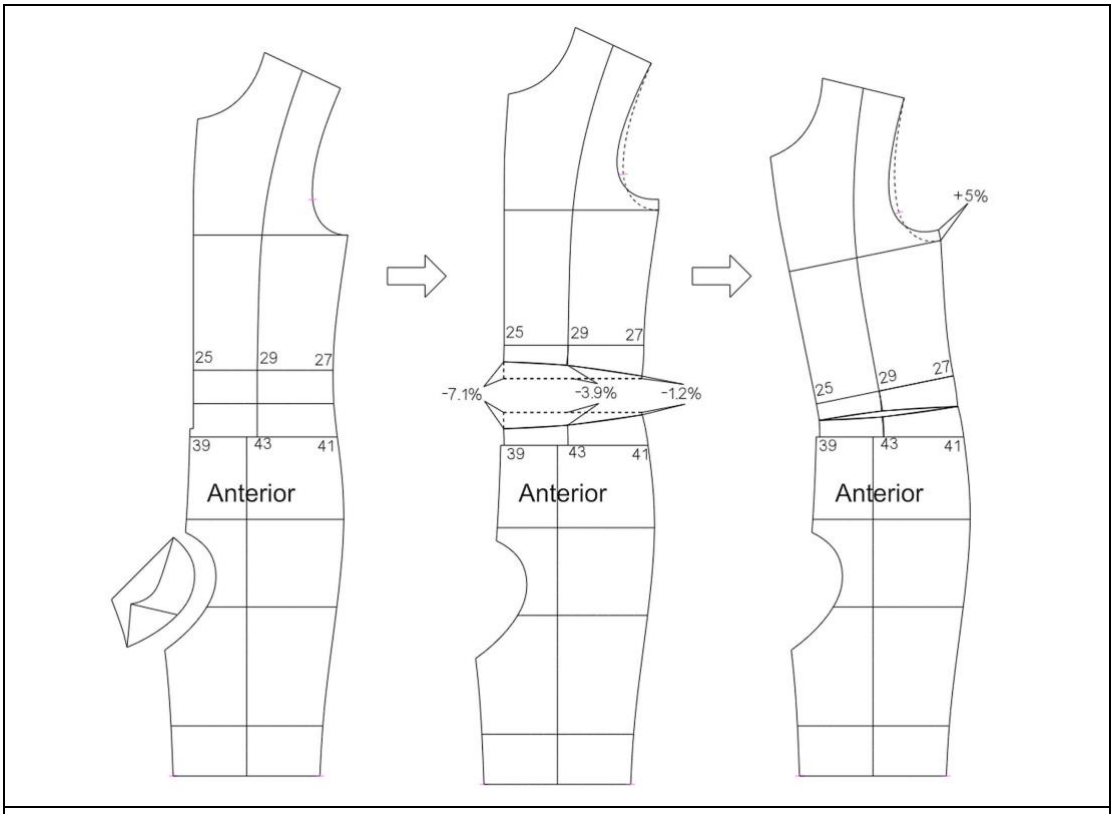

Figure 7. Longitudinal adjustment of ease rates for the CCS anterior pattern

Solid line, the adjusted CCS pattern.

Sleeve pattern

The armhole depth was decreased by around 5% in bending posture when compared to the armhole in standing posture (see Figure 8). Therefore, Figures 8 and 9 show the skin deformation rate transformed on posterior and anterior CCS pattern adjustment of 5% increment of the side seams.

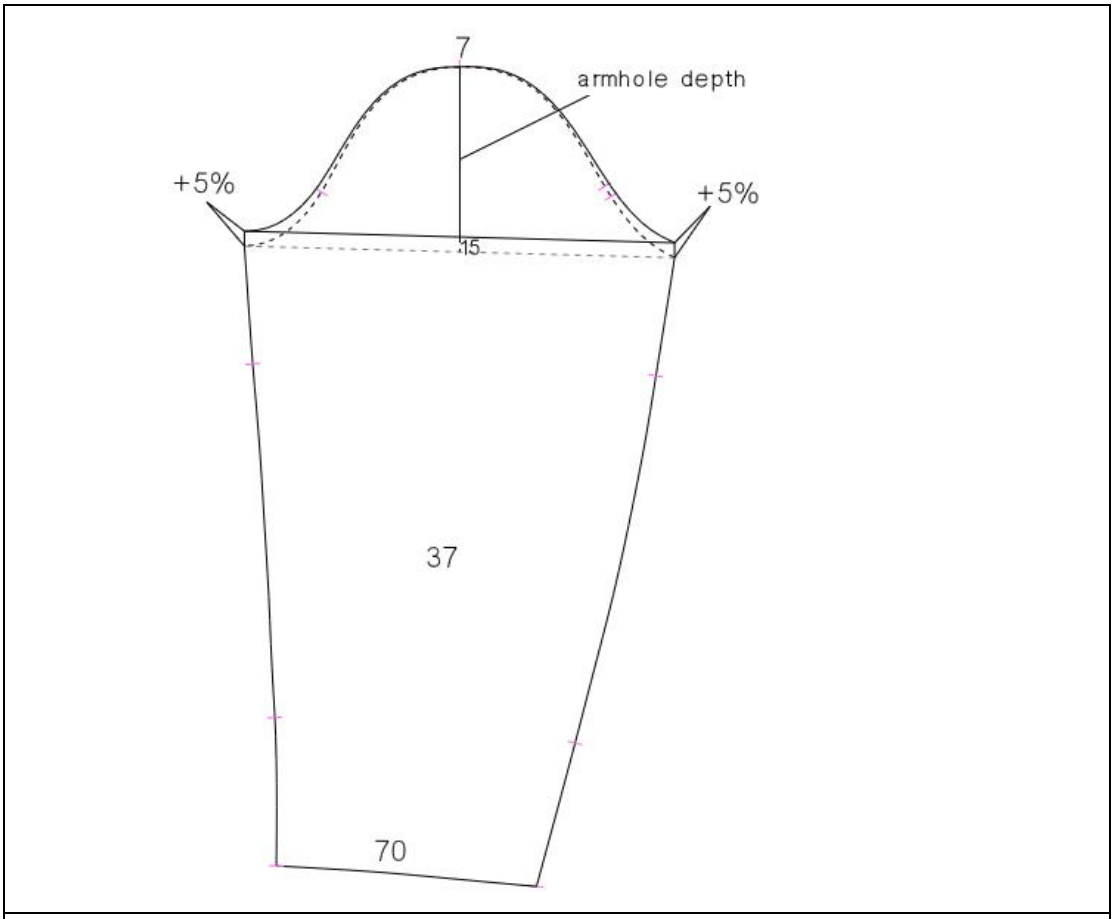

Figure 8. Longitudinal adjustment of ease rates for the CCS sleeve pattern

Solid line, the adjusted CCS pattern.

Transverse adjustment rates of the CCS pattern

Table 5 and Figure 9 show transverse adjustment rates of the CCS pattern. Based on skin deformation result, the width of posterior pattern was increased, and the maximum increase of the pattern was placed at posterior interscye length (F) by 24%. The whole circumference of waist was increased by 12% during cycling in a bending posture. The width of the anterior pattern was decreased at the middle center and anterior chest areas to reduce the bulky wrinkle during cycling in a bending posture.

Table 5. Transverse direction analysis for the CCS torso pattern.

Items	ID	Skin deformation (%)	Ease rate (%)
Ant. neckbase C	D’	-4.7	(Ant. neckbase C * 80%) – (Ant. neckbase C * 80%) * (4.7%)
Post. neckbase C	D	6.7	(Post. neckbase C * 80%) – (Post. neckbase C * 80%) * (6.7%)

Ant. biacromial W	E’	-18.7	(Ant. biacromial W * 80%) – (Ant. biacromial W * 80%) * (18.7%)
Post. biacromial W	E	7.6	Post. biacromial W * 80% + (Post. biacromial W * 80%) * 7.6%
Half ant. upper chest L	F’	-15.8	Half ant. upper chest L * 80% - (Half ant. upper chest L * 80%) * (15.8%)
Post. interscye L	F	32.0	Post. interscye L * 80% + (Post. interscye L * 80%) * 32%
Ant. waist C	G’	3.1	(Ant. waist C + Post. waist C) * 80%
Post. waist C	G	9.6	+ (waist C * 80%) * 12.7%
Ant. pant waist C	H’	-0.3	0%
Post. pant waist C	H	-0.5	0%

Ant.: anterior; C: circumference; L: length; Post.: posterior; W: width.

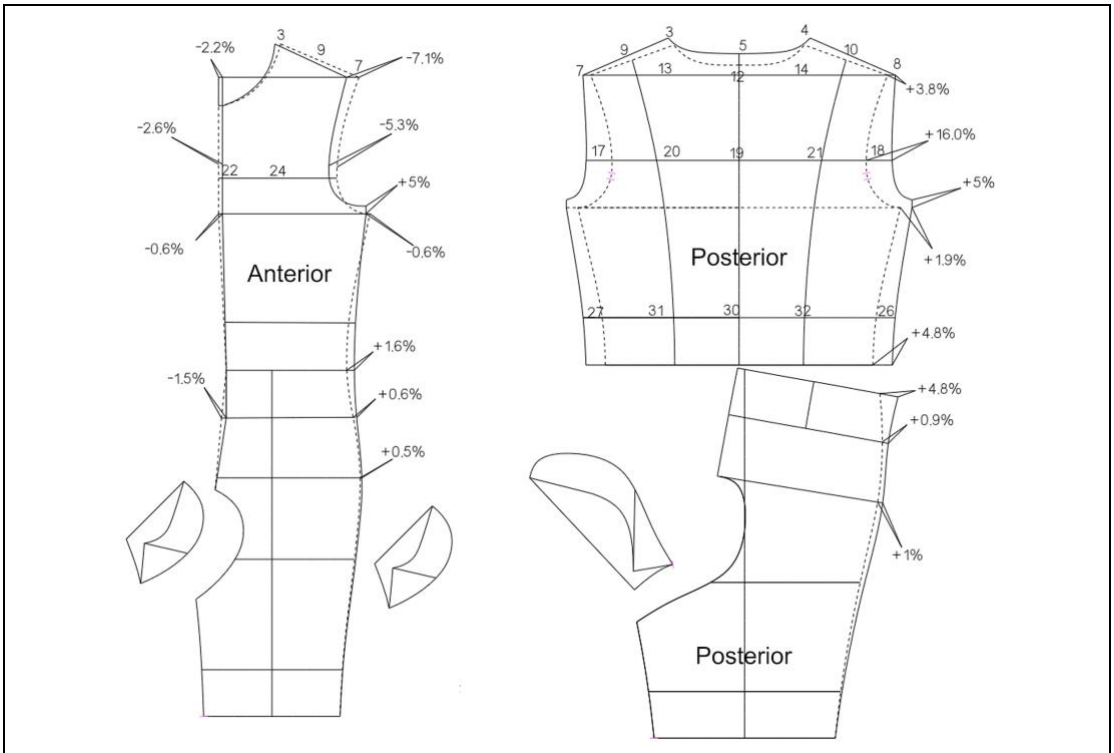

Figure 9. Transverse adjustment of ease rates for the CCS pattern

Solid line, the adjusted CCS pattern.

Diagonal adjustment rates of the CCS pattern

Figure 10 shows the diagonal adjustment of the CCS pattern. The adjustment trend of the diagonal direction is the same as the other two directions. The anterior diagonal lines of the pattern were decreased, whilst the posterior diagonal lines were increased.

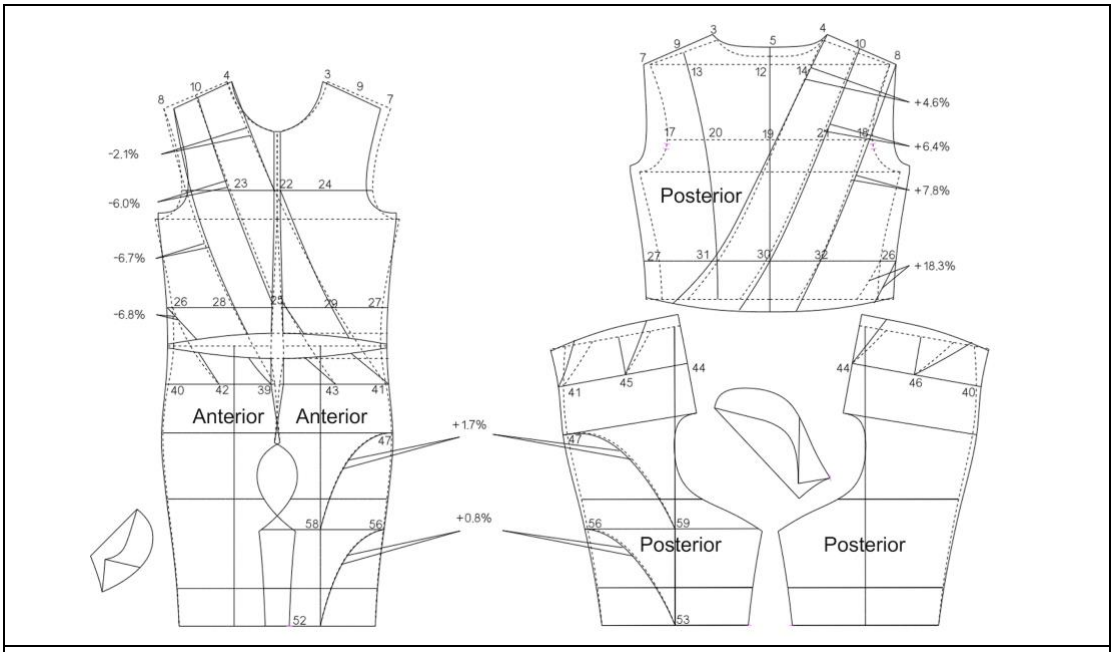

Figure 10. Diagonal adjustment of ease rates for the CCS pattern

Solid line, the adjusted CCS pattern.

Figure 11 shows the new CCS pattern for cycling in a bending posture. The change rates and points visually present the pattern differences between cycling in a bending posture and a standing posture.

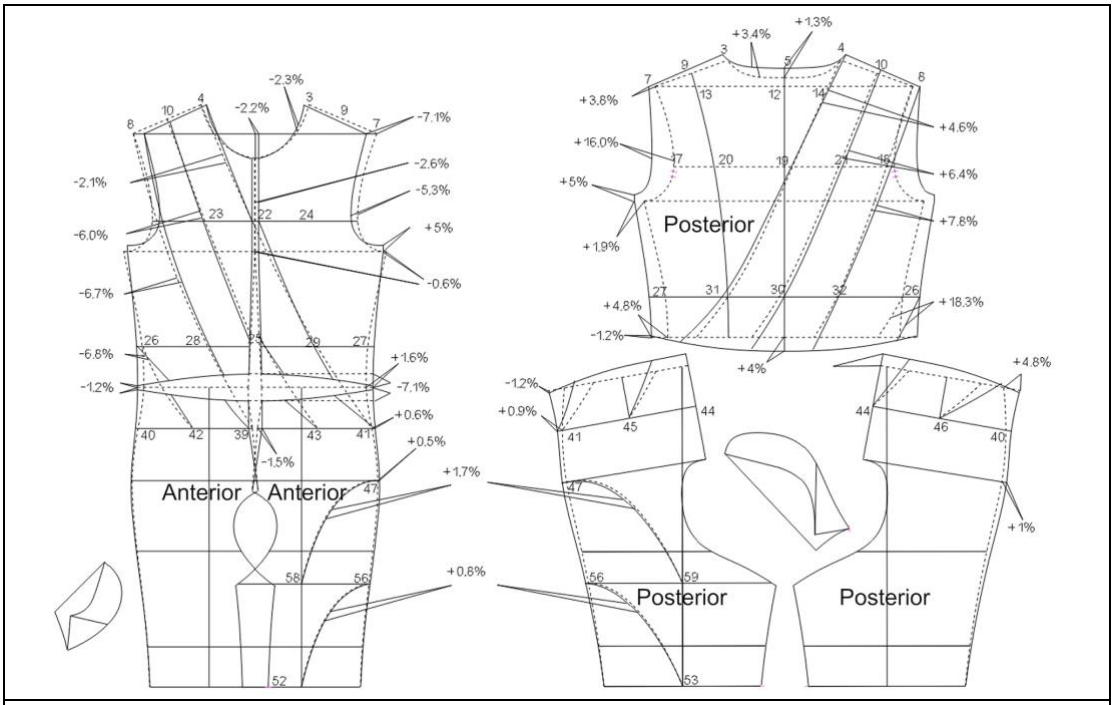

Figure 11. The CCS pattern for cycling in a bending posture

Solid line, the adjusted CCS pattern.

Discussion

This study assumed that skin deformation is essential for the next-to-skin functional skinsuit design, especially for loose fabric and wrinkle reduction, which is crucial for aerodynamic drag diminution. In this study, the deformation of skin lines on both torso and thigh were studied from three directions during an entire cycling motion in bending posture by a twelve cameras motion capture system. The skin deformation during pedaling was acquired and applied on the CCS pattern adjustment.

The skin deformation of the torso during cycling in bending posture was first investigated in this study, since previous studies (7, 10, 27, 28) investigated only the lower body's skin deformation. The results from the studies by Choi (7, 10) showed that skin deformation (i.e., contraction and extension) of the anterior and the posterior were opposite during cycling in bending posture. However, the skin formation data used in these two studies were captured during sitting instead of dynamic cycling in a bending posture. The skin deformation varies in different sport types, so the motion analysis should be applied for the specific sport instead of static simulation postures. Wang et al. (29) did an experiment for skin deformation analysis in static simulation postures of cycling. The mean of ten subjects' posterior center length was increased by

9.88% in which the waist was bending forward by a 90 degrees' posture, and the result of posterior center length in this study was similar which was increased by 9.27% during cycling in a bending posture. However, the mean deformation of anterior center length was extended by 9.35% (29). Oppositely, the mean of anterior center length in this study was compressed by 14.17%. This difference might because the bending forward posture instead of cycling bending posture was adopted in the study by Wang et al. (29). Although skin deformation of the torso was consistent and only changed with the breathing during cycling in bending, it is still essential to acquire the accurate deformation rate which relates to aerodynamic drag during cycling.

The study of skin deformation during cycling is very limited. The knee flexion angle range during cycling was found to be between 73° and 137° in this study. The skin deformation of the thigh reached a minimum when peddling was at the BDC position with the maximum knee flexion angle, while the deformation rate was increased to the maximum when peddling was at the TDC position with the minimum knee angle during cycling in a bending posture. This finding is similar to that of Luo et al. (28) in their study. In this study, it was also found that the change rates of longitudinal skin lines on the anterior and posterior thigh were higher than the skin lines in another two directions. Most of previous studies studied skin deformation at 0°, 30°, 45°, 60°, 90°, 120° knee flexion angles for running compression tights application. The results of those studies could be considered as useful information for pattern construction. However, different sports involve different muscle groups, with corresponding variations of skin deformation during the sport exercise. Although parts of knee flexion angles applied in previous studies were in cycling knee flexion range, without saddle height and cycling posture considerations, the factors of pedal forces, saddle height, and kinematics which affect muscle deformation were missing, whilst those factors will be different in constant dynamic exercise from active postures, which lead to the different skin deformation results among studies. The more detailed skin deformation values can provide more specific information for ease amounts to achieve better fit and reduce aerodynamic drag for CCS. The results of skin deformation rates were applied on CCS pattern adjustment to help the cyclists save more energy with better fitting and less aerodynamic drag. The method and results of skin deformation by motion capture in this study could be used as a useful reference for the cycling garment industry. This study was, however, conducted with a small number of subjects so the results cannot be generalized to represent a wider population. Another limitation of this study was that

the reflective markers at hip area were not captured. Thus, another method to capture 3D skin deformation data of the hip area during cycling should be considered for future study.

Conclusion

The skin deformation of the torso during cycling in bending posture was the focus in this study. The skin lines on the anterior were compressed, while those on the posterior were extended from three directions during cycling in a bending posture when compared with a standing posture. The adjusted CCS according to the method introduced in this study has been proven to facilitate the cyclists to reduce energy consumption during cycling (19, 30). The visualized dynamic 3D skin deformation analyzed through a motion capture system including kinetic (i.e., pedal force) and kinematic considerations in this study can be provided as a guideline for CCS or other compression garment pattern design.

Data Availability

Data are available upon reasonable request.

Conflict of interest

The authors declare that they have no conflicts of interest.

Funding statement

This research is funded by (details omitted for double-anonymous peer review).

References

1. Oggiano L, Troynikov O, Konopov I, Subic A, Alam F. Aerodynamic behaviour of single sport jersey fabrics with different roughness and cover factors. Sports Engineering. 2009;12(1):1-12.
2. Bracey J. Do you need an aerosuit for road riding? Cycling Weekly. 2016.
3. Swart J, Holliday W. Cycling Biomechanics Optimization-the (R) Evolution of Bicycle Fitting. Curr Sports Med Rep. 2019;18(12):490-6.
4. Malizia F, Blocken B. Cyclist aerodynamics through time: Better, faster, stronger. Journal of Wind Engineering and Industrial Aerodynamics. 2021;214:104673.
5. Wang Y, Li H, Li J. The skin deformation during cycling on terrains for practical application of compression sportswear. The Journal of The Textile Institute. 2021;112(5):691-9.
6. Petrova A, Ashdown S. Three-Dimensional Body Scan Data AnalysisBody Size and Shape Dependence of Ease Values for Pants' Fit. Clothing and Textiles Research Journal. 2008;26:227-52.
7. Choi S, Ashdown SP. 3D body scan analysis of dimensional change in lower body measurements for active body positions. Textile Research Journal. 2010;81(1):81-93.
8. Lee H, Hong K, Lee Y. Ergonomic mapping of skin deformation in dynamic postures to provide fundamental data for functional design lines of outdoor pants. Fibers and Polymers. 2013;14(12):2197-201.
9. Seo H, Kim S-j, Cordier F, Choi J, Hong K. Estimating dynamic skin tension lines in vivo using 3D scans. Computer-Aided Design. 2013;45(2):551-5.
10. Choi J, Hong K. 3D skin length deformation of lower body during knee joint flexion for the practical application of functional sportswear. Appl Ergon. 2015;48:186-201.
11. Lukes RA, Chin SB, Haake SJ. The understanding and development of cycling aerodynamics. Sports Engineering. 2005;8(2):59-74.
12. Bini R, Hume PA, Croft JL. Effects of bicycle saddle height on knee injury risk and cycling performance. Sports Med. 2011;41(6):463-76.
13. Sanderson DJ, Amoroso AT. The influence of seat height on the mechanical function of the triceps surae muscles during steady-rate cycling. J Electromyogr Kinesiol. 2009;19(6):e465-71.
14. Bini R. Influence of saddle height in 3D knee loads commuter cyclists: A statistical parametric mapping analysis. J Sports Sci. 2021;39(3):275-88.

15. Brochard S, Lempereur M, Remy-Neris O. Double calibration: an accurate, reliable and easy-to-use method for 3D scapular motion analysis. J Biomech. 2011;44(4):751-4.
16. Hussain SH, Limthongkul B, Humphreys TR. The biomechanical properties of the skin. Dermatol Surg. 2013;39(2):193-203.
17. Defraeye T, Blocken B, Koninckx E, Hespel P, Carmeliet J. Aerodynamic study of different cyclist positions: CFD analysis and full-scale wind-tunnel tests. J Biomech. 2010;43(7):1262-8.
18. Balasubramanian V, Jagannath M, Adalarasu K. Muscle fatigue based evaluation of bicycle design. Appl Ergon. 2014;45(2):339-45.
19. Shi Q. Compression cycling garment design for performance enhancement and muscle fatigue recovery: The Hong Kong Polytechnic University; 2020.
20. Kouchi M, Mochimaru M. Errors in landmarking and the evaluation of the accuracy of traditional and 3D anthropometry. Appl Ergon. 2011;42(3):518-27.
21. Troynikov O. 3D Body Scanning Method for Close- Fitting Garments in Sport and Medical Applications. HFESA 47th Annual Conference 2011 11 (16), 1-6. 2011;11:1-6.
22. Gayzik FS, Moreno DP, Danelson KA, McNally C, Klinich KD, Stitzel JD. External landmark, body surface, and volume data of a mid-sized male in seated and standing postures. Ann Biomed Eng. 2012;40(9):2019-32.
23. Kouchi M. 3 - Anthropometric methods for apparel design: body measurement devices and techniques. In: Gupta D, Zakaria N, editors. Anthropometry, Apparel Sizing and Design: Woodhead Publishing; 2014. p. 67-94.
24. ISO 7250-1, Basic human body measurements for technological design— Part 1: Body measurement definitions and landmarks. 2017.
25. Greenberg SA. The history of dermatome mapping. Arch Neurol. 2003;60(1):126-31.
26. Silberman MR, Webner D, Collina S, Shiple BJ. Road bicycle fit. Clin J Sport Med. 2005;15(4):271-6.
27. So RCH, Ng JKF, Ng GYF. Muscle recruitment pattern in cycling: a review. Physical Therapy in Sport. 2005;6(2):89-96.
28. Luo S, Wang J, Yao X, Zhang L. A novel method for determining skin deformation of lower limb in cycling. The Journal of The Textile Institute. 2017;108(9):1600-8.

29. Wang YJ, Mok PY, Li Y, Kwok YL. Body measurements of Chinese males in dynamic postures and application. Applied Ergonomics. 2011;42(6):900-12.
30. Shi GQQ, Shin K, Chow DHK, Jiao J, So BCL, Lau N, et al. Influences of compression cycling skinsuit on energy consumption of amateur male cyclists. Textile Research Journal. 2021;92(15-16):2697-710.